



Influence of interaction between small asperities on various types of slow earthquakes in a 3-D simulation for a subduction plate boundary

Keisuke Ariyoshi^{a,*}, Takane Hori^a, Jean-Paul Ampuero^b, Yoshiyuki Kaneda^a, Toru Matsuzawa^c, Ryota Hino^c, Akira Hasegawa^c

^a Department of Oceanfloor Network System Development for Earthquakes and Tsunamis (DONET), Japan Agency for Marine-Earth Science and Technology (JAMSTEC), Yokohama 236-0001, Japan

^b Seismological Laboratory, California Institute of Technology, Pasadena, California 91125-2100, USA

^c Research Center for Prediction of Earthquakes and Volcanic Eruptions, Graduate School of Science, Tohoku University, Sendai 980-8578, Japan

ARTICLE INFO

Article history:

Received 15 November 2008
Received in revised form 6 March 2009
Accepted 7 March 2009
Available online 27 March 2009

Keywords:

Non-volcanic deep low-frequency tremors
Slow slip events
Rupture propagation process
Chain reaction
Rate and state dependent friction law

ABSTRACT

Recently, the occurrence of slow earthquakes such as low-frequency earthquakes and very low-frequency earthquakes have been recognized at depths of about 30 km in southwest Japan and Cascadia. These slow earthquakes occur sometimes in isolation and sometimes break into chain-reaction, producing tremor that migrates at a speed of about 5–15 km/day and suggesting a strong interaction among nearby small asperities. In this study, we formulate a 3-D subduction plate boundary model with two types of small asperities chained along the trench at the depth of 30 km. Our simulation succeeds in representing various types of slow earthquakes including low-frequency earthquakes and rapid slip velocity in the same asperity, and indicates that interaction between asperities may cause the very low-frequency earthquakes. Our simulation also shows chain reaction along trench with propagation speed that can be made consistent with observations by adjusting model parameters, which suggests that the interactions also explain the observed migration of slow earthquakes.

© 2009 International Association for Gondwana Research. Published by Elsevier B.V. All rights reserved.

1. Introduction

Owing to dense networks of high sensitive seismic stations, low-frequency earthquakes have been detected in the southwestern part of Japan at a depth of about 30 km (Obara, 2002) on the subduction plate boundary (Shelly et al., 2006), where slow slip events also have been detected by GPS networks (Hirose and Obara, 2005), and there are large, strong asperities such as Tokai, Tonankai, Nankai earthquakes on the shallower part of subducting plate boundary above the depth of 30 km (e.g., Obara, 2002). Ito et al. (2007) found that not only low-frequency earthquakes but also very low-frequency earthquakes occur in the same region, and suggested that the asperity size of very low-frequency earthquake is larger than that of low-frequency earthquake. However, it has not been clear from hypocenter determination studies that the locations of low-frequency earthquakes are always different from those of very low-frequency earthquakes. Ide et al. (2007) categorized low-frequency earthquake, very low-frequency earth-

quake, slow slip event and episodic tremor and slip as a group named “slow earthquakes” with similar scaling relation in different scale of duration time (e.g., slow slip event: several days to years, low-frequency earthquake: several tens of seconds to several days). Since slow slip events are accompanied by low-frequency earthquakes as observed in Bungo channel region, southwest Japan (Hirose and Obara, 2005), slow slip events may be composed of some groups of low-frequency earthquakes and/or very low-frequency earthquakes.

Some low-frequency earthquakes seem to migrate along trench at rates of 5–15 km/day in Cascadia (Rogers and Dragert, 2003) and 10–13 km/day in southwestern Japan (Obara, 2002; Obara and Hirose, 2006). Obara (2002) suggested that this migration is caused by the movement of fluid dehydrated from the slab, but it is still unclear whether fluid flow over several tens of kilometers is a necessary condition for the migration of low-frequency earthquakes.

Slow slip transients and their propagation processes have been explained by numerical simulation studies based on rate- and state-dependent friction laws. Liu and Rice (2005) succeeded in reproducing important aspects of aseismic slip transients, by introducing along-strike variations of constitutive parameters or non-uniform initial conditions to excite the non-uniform slip patterns that are intrinsic to spatially homogeneous fault models with large aspect

* Corresponding author. Tel.: +81 45 778 5450.
E-mail address: ariyoshi@jamstec.go.jp (K. Ariyoshi).

ratio (Horowitz and Ruina, 1989; Hirose and Hirahara, 2002). Inhomogeneity of friction parameters may also affect the migration of low-frequency earthquakes. Shibazaki and Shimamoto (2007) represented short-interval slow slip events by considering the frictional behavior of the unstable-stable transition regime at high slip velocity. The friction law has a significant influence on models of slow slip event.

On the other hand, Matsuzawa et al. (2004) proposed that aseismic afterslip is propagated by a chain reaction of rupturing asperities. We suggest that this process may also explain the along-trench propagation of low-frequency earthquakes or very low-frequency earthquakes. In this study, we investigate whether interaction between small asperities along the trench can explain the various types of slow earthquakes and their migration processes by numerical simulations of subduction plate boundary models based on a rate- and state-dependent friction law, comparing our simulation results to other studies.

2. Numerical model

The three-dimensional (3D) numerical simulation employed in the present study is similar to that described by Liu and Rice (2005) and Ariyoshi et al. (2007a). The model considers a planar plate interface dipping at 15° from the free surface in a half-space homogeneous elastic medium (Fig. 1a) with periodic boundary condition along the strike direction. The plate interface is divided into 1024 (strike) × 195 (dip) cells. Slip is assumed to be pure dip and to obey the quasi-static equilibrium between shear and frictional stresses:

$$\mu_i \sigma_i = \sum_{j=1}^N K_{ij} (u_j(t) - V_{pl} t) - \frac{G}{2\beta} \frac{du_i}{dt}, \quad (1)$$

Here, the subscripts i and j denote the location indices of an observation and a source cell, respectively. Eq. (1) describes the stress in the i -th cell caused by dislocations, where V_{pl} is the relative speed of the two plates, t denotes time, N is the total number of cells, G is rigidity, β is the shear wave speed, and K_{ij} is the Green's function for shear stress (Okada, 1992) on the i -th cell. K_{ij} is calculated from the quasi-static solution for uniform pure dip-slip u relative to average slip $V_{pl} t$ (Savage, 1983) over a rectangular dislocation in the j -th cell. The first term of the right-hand side has the form of a convolution. The fast Fourier transform can be used for analysis of the along-strike component because the Green's function K_{ij} for the strike component is dependent on the relative distance between the observation and source points (Rice, 1993). The last term in Eq. (1) is introduced to incorporate radiation damping (Rice, 1993).

In Eq. (1), the effective normal stress σ is given by

$$\sigma_i(z) = \kappa(z)(\rho_{rock} - \rho_w)gz, \quad (2)$$

where ρ_{rock} and ρ_w are the densities of rock and water, respectively, g is acceleration due to gravity, and z is depth. The function $\kappa(z)$ is a super-hydrostatic pore pressure factor as given in Fig. 1b, which assumes that a high pore pressure system locally exists around 30 km depth due to the dehydration derived from facies change in the slab (e.g., Kita et al., 2006; Hasegawa et al., 2007) which has been clearly monitored by tomography studies (e.g., Zhao et al., 2007; Sun et al., 2008; Zhao, 2009; Zhao and Ohtani, 2009-this issue) and geological investigations (e.g., Kutsukake, 2002; see also Mishina, 2009-this issue on resistivity surveys to detect fluid reservoirs). Ariyoshi et al. (2007b) estimate that the value of κ is 0.1 for the deeper part (>30 km depth) on the basis of afterslip propagation speed. Wang and Suyehiro (1999) suggest that the apparent frictional coefficient is about 0.03 from stress field observation in northeastern and southwestern Honshu, Japan, which is consistent with $\kappa = 0.1$.

The friction coefficient μ in Eq. (1) is assumed to obey a rate- and state-dependent friction law (Dieterich, 1979; Ruina, 1983), as given by

$$\mu_i = \mu_0 + a_i \log(V_i / V_0) + b_i \log(V_0 \theta_i / d_{ci}), \quad (3)$$

$$d\theta_i / dt = 1 - V_i \theta_i / d_{ci}, \quad (4)$$

where a and b are friction coefficient parameters, d_c is the characteristic slip distance associated with b , θ is a state variable for the plate interface, V is slip velocity, and μ_0 is a reference friction coefficient defined at a constant reference slip velocity of V_0 .

Eqs. (1), (3), (4) are solved using the Runge–Kutta method with adaptive step-size control (Press et al., 1996). The constant parameters common to all models tested here are: $G = 30$ GPa, $\beta = 3.75$ km/s, $g = 9.8$ m/s², $\rho_{rock} = 2.75 \times 10^3$ kg/m³, $\rho_w = 1.0 \times 10^3$ kg/m³, $V_0 = 1$ μ m/s, $\mu_0 = 0.6$, Poisson's ratio $\varepsilon = 0.25$, and $V_{pl} = 4.0 \times 10^{-2}$ m/yr or 1.3×10^{-9} m/s.

Frictional stability is usually represented by $\gamma = a - b$. If $\gamma > 0$, frictional stress increases with sliding velocity, similar to viscous coupling. If $\gamma < 0$, frictional stress decreases with increasing sliding velocity, resulting in stick-slip behavior (Ruina, 1983). In the present paper, an asperity denotes a region with $\gamma < 0$, following Boatwright and Cocco (1996). The plate interface is demarcated into five regions, as shown in Fig. 1b: (i) large asperity (LA) region, (ii) ten middle asperity (MA) regions, (iii) twenty small asperity (SA) regions, (iv) weakly stable region (WS), and (v) strongly stable region (SS). The frictional parameters shown in Fig. 1c are based on rock laboratory results (e.g., Blanpied et al., 1998): $(a_1, a_2) = (2, 5) [\times 10^{-3}]$; frictional stability parameters, $(\gamma_1, \gamma_2, \gamma_3) = (-0.4, 0.01, 4.0) [\times 10^{-3}]$; and characteristic slip distances, $(d_{c1}, d_{c2}, d_{c3}) = (40, 1.0, 0.5) [\times 10^{-3}]$ m. The asperity radii take the following values: for MA, $(R_1, R_2, R_3) = (4.0, 4.5, 5.0)$ [km]; for SA, $(r_1, r_2, r_3) = (2.0, 2.25, 2.5)$ [km]; for longer radii of LA, $(L_1, L_2, L_3) = (90, 95, 100)$ [km] with aspect ratio 0.38. The distance between central points of SA and MA is 5 and 10 km, respectively, so as to be adjacent each SA and MA, which is to be discussed later.

The sizes of the cells h_i in the asperities are set such that all cells in LA, MA and SA are at least 5.2 times smaller than the critical cell size $h^* = \eta G d_c / \sigma (b - a)$, where $\eta = K_{ii} h_i / G$ is a geometrical factor (Rice, 1993). A smaller critical cell size $L_b = \eta G d_c / \sigma b$ has been recently proposed on the basis of numerical simulations and analytical results (Rubin and Ampuero, 2005; Perfettini and Ampuero, 2008) and adopted in other simulation studies (e.g., Shibazaki and Shimamoto, 2007; Ziv, 2007). At the center of LA, MA and SA, $(L_b^{\text{strike}}, L_b^{\text{dip}})$ is (1.6, 5.8), (0.35, 0.31) and (0.17, 0.16) [km], respectively. Though the cell size of SA along strike and dip direction (0.20, 0.17) [km] is slightly larger than L_b , by reducing the cell size by half we did not find significant qualitative differences in the simulation results discussed next.

3. Simulation results

3.1. Overview of the evolution of stress drop and slip velocity for SA and MA

We uniformly set the initial shear stress at the steady state friction value at a rate of $0.9 V_{pl}$. Fig. 2 shows (a, c, e, g, i) frictional coefficient (or shear stress normalized by the effective normal stress) and (b, d, f, h, j) slip velocity normalized with respect to V_{pl} on a common-logarithmic scale averaged in each asperity No. 28–31 (SA) and No. 2–5 (MA) as named in Fig. 1b. The origin time in Fig. 2a–b is one hundred years after the initial conditions, after the first large event of LA. The frequency of slip and stress drop events per decade shown in Fig. 2a–b is about 12–20 for SA and 6–9 for MA, which corresponds to recurrence intervals of 0.5–

0.8 year for SA and 1.1–1.7 years for MA. On the other hand, the recurrence interval of LA is about 180 years.

Since recurrence intervals of SA and MA are short and slip events occur at some asperities most of time, the adaptive time step of the Runge–Kutta method tends to remain small and the computation cost for several slip cycles of LA becomes huge. In this study, we focus mainly on the preseismic stage of LA, where a giant earthquake occurs at LA after 27 years from the end time of Fig. 2a–b, to investigate the stress shadow effect of LA and avoid the heavy calculation cost. In order to validate the simulation results, we performed simulations with different initial conditions and cell sizes and found that our simulation results are not affected by such conditions.

From GPS data analyses for slow slip events in Cascadia, recurrence interval, maximum slip velocity and shear stress drop are estimated to be 14 months (Miller et al., 2002), 1 m/yr (3.2×10^{-8} m/s) and 0.04–0.06 MPa (Miyazaki et al., 2006), respectively. In our simulation, the slip velocity averaged in MA and SA is in the range 10^{-8} – 10^{-6} m/s as shown in Fig. 2b, and stress drops of slip events in SA and MA are in the range 0.02–0.08 MPa from Fig. 2a, where the effective normal stress in Eq. (1) at 30 km depth is 51 MPa. These simulation results are quantitatively consistent with the observational results in case of constant stress drop model. Therefore, we basically refer to these slip events in our simulation as slow earthquakes in our simulation. Since the size and frictional properties of asperities are common within the SA and MA groups, the fluctuations of the slow earthquake properties seem to be induced by the interaction between the small asperities (MA and SA).

To examine the interaction processes, we select and investigate four characteristic patterns of slow earthquakes by snapshots of slip velocity in the following sections. Note that some slip events have averaged slip velocities several orders of magnitude greater ($\sim 10^{-5}$ m/s), including areas of coseismic slip ($> 10^{-2}$ m/s), and averaged shear stresses several times greater (~ 0.16 MPa) than the observed low-frequency earthquakes and more similar to regular earthquakes. Some other slip events have lower slip velocity with longer duration time than usual low-frequency earthquakes, and are more similar to very low-frequency earthquakes (Ito et al., 2007; Ide et al., 2007). Their slip process and propagation speed is similar to one of the following characteristic patterns.

3.2. Comparison of propagation process between MA and SA

As an example of chained propagation process of slow earthquakes in MA, Fig. 3 shows a time-series of snapshots of slip velocity normalized by V_{pl} on a common-logarithmic scale from 0.16 year in Fig. 2c–d (blue background). It is common in Fig. 3 that small slip events continuously occur above LA. This is due to the shear stress gap derived from slip relative to V_{pl} in Eq. (1) between LA ($u(t) - 0$) and the outside of trench ($u(t) - V_{pl}t$; Savage, 1983), and temporally prominent when the distance from the trench to the strongly locked region around LA is short. Therefore, this behavior is artificial. It is needed for our future study to remove the artificial slip behavior by improving our model, though we found that this artificial behavior seems not to affect the character of various types of deep slow earthquakes as seen in Figs. 4–6 explained later.

In Fig. 3, unilateral chained propagation process is clearly seen for MA, with propagation speed between asperities No. 7 to No. 5 of about 0.2 km/day (Fig. 3b–d). In the time span indicated by the blue background in Fig. 2c–d, the patterns of stress drop and averaged slip

velocity at asperities No. 3 to 5 appear to be relatively similar but quantitatively different. Especially, the amount of stress drop and averaged slip velocity in asperity No. 3 is greater than in the others. In Fig. 3b–d, there is not only leftward chained propagation from the asperity No. 10 but also rightward propagation from the asperity No. 2, where the latter is much slower than the former because of the large area locked in the asperity No. 3. In Fig. 3e, both chained propagations cross at the asperity No. 3, which promotes larger stress drop and higher slip velocity. Since similar behavior seems to be seen in the simulation of Liu and Rice (2005), these results suggests that some phenomena generated by introducing along-strike variations of constitutive parameters or non-uniform initial conditions may be represented by interaction between small asperities.

On the other hand, the propagation process of SA is different from that of MA in some respects. Fig. 4 shows leftward propagation from the asperity No. 2 through No. 31 to No. 22, which is due to the periodic boundary condition. In the time span indicated by a green background in Fig. 2e–f there are two slow earthquakes for each asperity from No. 28 to 31. Propagation speed between asperities No. 31 to 28, No. 28 to 23 and No. 23 to 22 is about 0.2, 0.15 and 0.03 km/day, respectively, which progressively becomes slower than that of MA. Fig. 4e shows that rightward propagation from the asperity No. 27 and 30 is also seen.

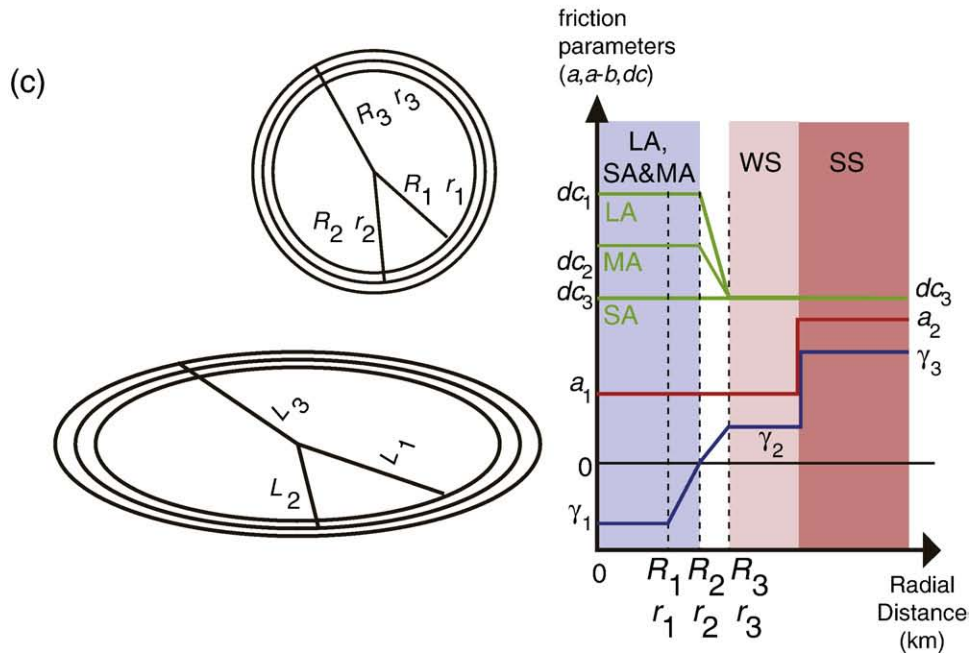
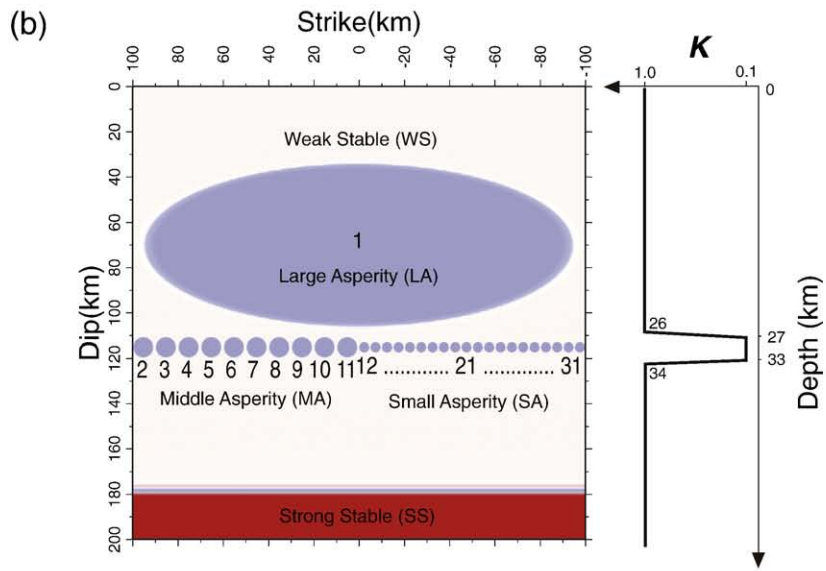
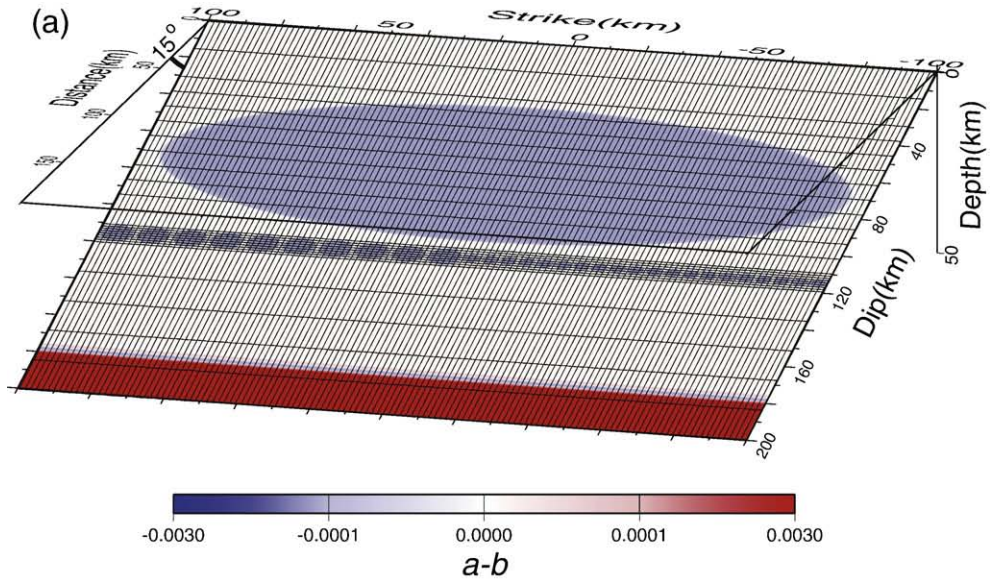
These differences from MA are explained as follows. SA has shorter recurrence intervals and smaller moment release because of smaller asperity size with shorter characteristic distance than those of MA. The smaller moment release makes propagation speed slower (0.03 km/day for SA is smaller than 0.2 km/day for LA), which causes that recurrence interval of SA is relatively much shorter than the passage time of aseismic slip across more than twice the SA diameters (10 km). In addition, locking of SA soon after the occurrence of slow earthquakes, due to their short characteristic distance, tends to prevent aseismic slip propagation. Therefore, slow earthquakes occur again soon after the passage of aseismic slip from asperity No. 29 as shown in Fig. 2e–f. This is why propagation process of SA as shown in Fig. 4e–f appears to be bilateral, rather than the unilateral propagation seen in Fig. 3.

3.3. Physical process of multiple ruptures and very low-frequency earthquake

Fig. 5 shows an example of a multi rupture process between asperities No. 3 to 5 in the time span indicated by a pink background in Fig. 2i–b). (ii) The velocity of preslip becomes locally higher (nearly red) around the center of asperity No. 5 and in the frictionally unstable region ($\gamma < 0$) between the centers of asperities No. 4 and 5 (Fig. 5c). (iii) A slow earthquake occurs in asperity No. 5 (Fig. 5d), and (iv) asperity No. 4 follows (Fig. 5e). (v) Afterslip of MA has enclosed the three asperities No. 3 to 5 (Fig. 5f). From Fig. 5d–e, the rupture speed from asperity No. 3 to 4 is roughly 3 km/day, which is significantly faster than that of Figs. 3 and 4. Slip propagation is promoted by the preslip of the slow earthquakes (warm colors in Fig. 5d–e) that has covered the area between the two asperities No. 3 and 4 in the dip range of 110–120 km. Therefore, a necessary condition for this multiple rupture is such synchronized preslip stage of slow earthquakes on each asperity as shown in Fig. 5b.

The series of snapshots in Fig. 6 show a case with no synchronization. Fig. 6a shows a pair of slow earthquakes at asperities No. 5 and 7, while Fig. 6b–c show a pair at asperities No. 4 and 6. After that, a slow

Fig. 1. (a) Schematic view of the 3-D simulation model of a plate boundary with frictional parameter $\gamma = a - b$. Note that the actual cell size in our simulation is more than eight times smaller than shown here. (b) Spatial distribution of LA, MA, SA ($\gamma < 0$) with identification numbers of the asperities, WS ($\gamma > 0$) and SS ($\gamma \gg 0$). Elevated pore pressure factor $\kappa(z)$ is drawn as a function of depth in the right side, where depth corresponds to dip in the left side. (c) Frictional parameters (a, γ, d_c) as functions of distance from the center of LA(L), MA (R) or SA(r), where $(L_1, L_2, L_3) = (90, 95, 100)$ [km] with aspect ratio 0.38, $(R_1, R_2, R_3) = (4.0, 4.5, 5.0)$ [km], $(r_1, r_2, r_3) = (2.0, 2.25, 2.5)$ [km], $(a_1, a_2) = (2, 5) [\times 10^{-3}]$, $(\gamma_1, \gamma_2, \gamma_3) = (-4.0, 0.1, 4.0) [\times 10^{-4}]$, and $(d_{c1}, d_{c2}, d_{c3}) = (40, 1.0, 0.5) [\times 10^{-3}$ m].



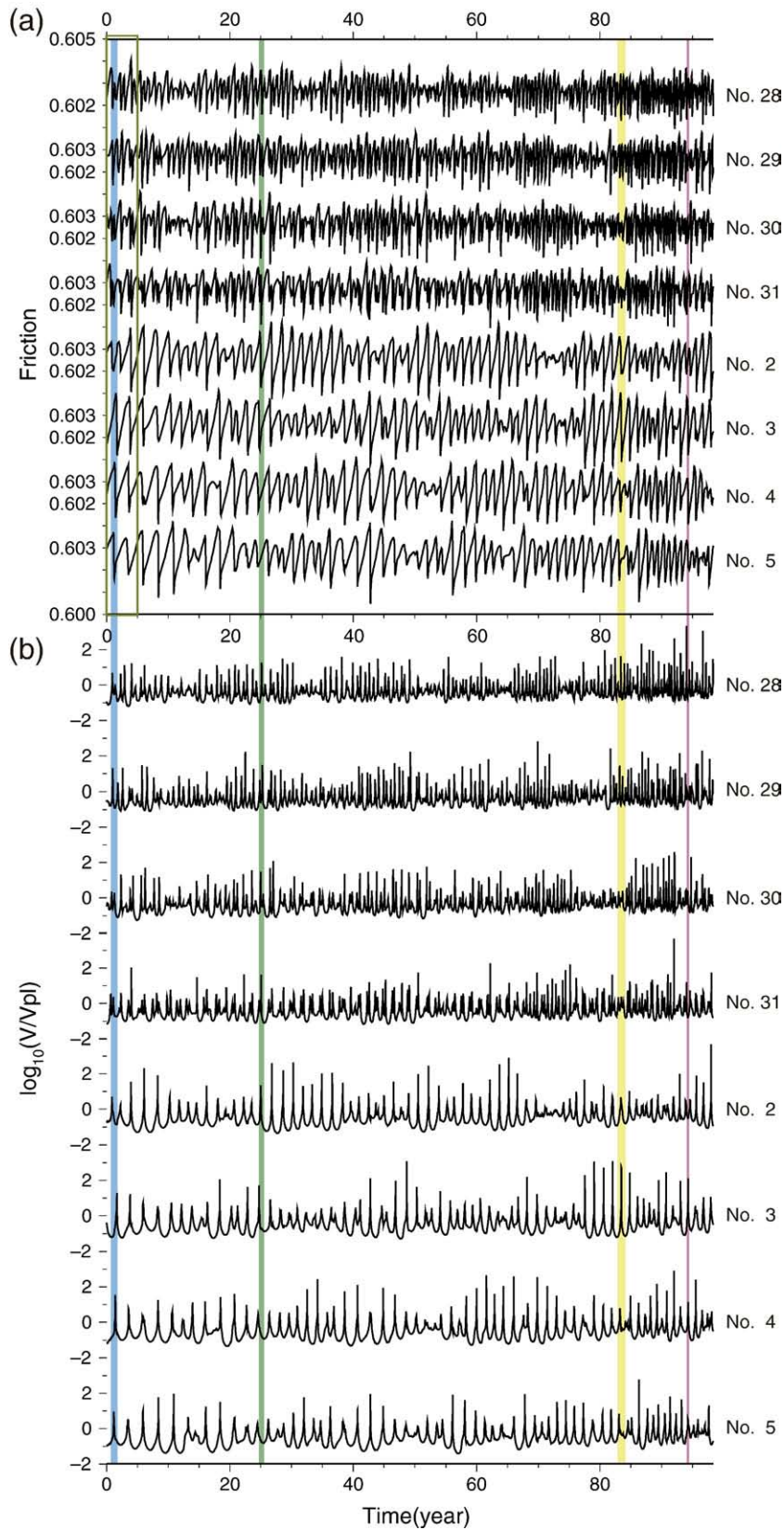


Fig. 2. Time histories of (a) friction coefficient and (b) common-logarithm of slip velocities averaged in the areas of MA or SA for asperities No. 2 to 5 and 28 to 31 as positioned in Fig. 1b. Time span marked by four (blue, green, yellow and pink) colors corresponds to the time series of snapshots in Figs. 3, 4, 6, 5, respectively. (c)–(j) Close-up of the time series before and after each snapshot.

earthquake occurs on asperity No. 3 (Fig. 6e), then slip propagates to the next asperity, No. 4 (Fig. 6f). In the time span indicated by a yellow background in Fig. 2g–h, some slow earthquakes with averaged slip

velocities nearly as low as V_{pl} have occurred at asperity No. 4, after the time of Fig. 6a, which is due to the short time for shear stress healing as shown in the friction history of Fig. 2g. This simulation result may

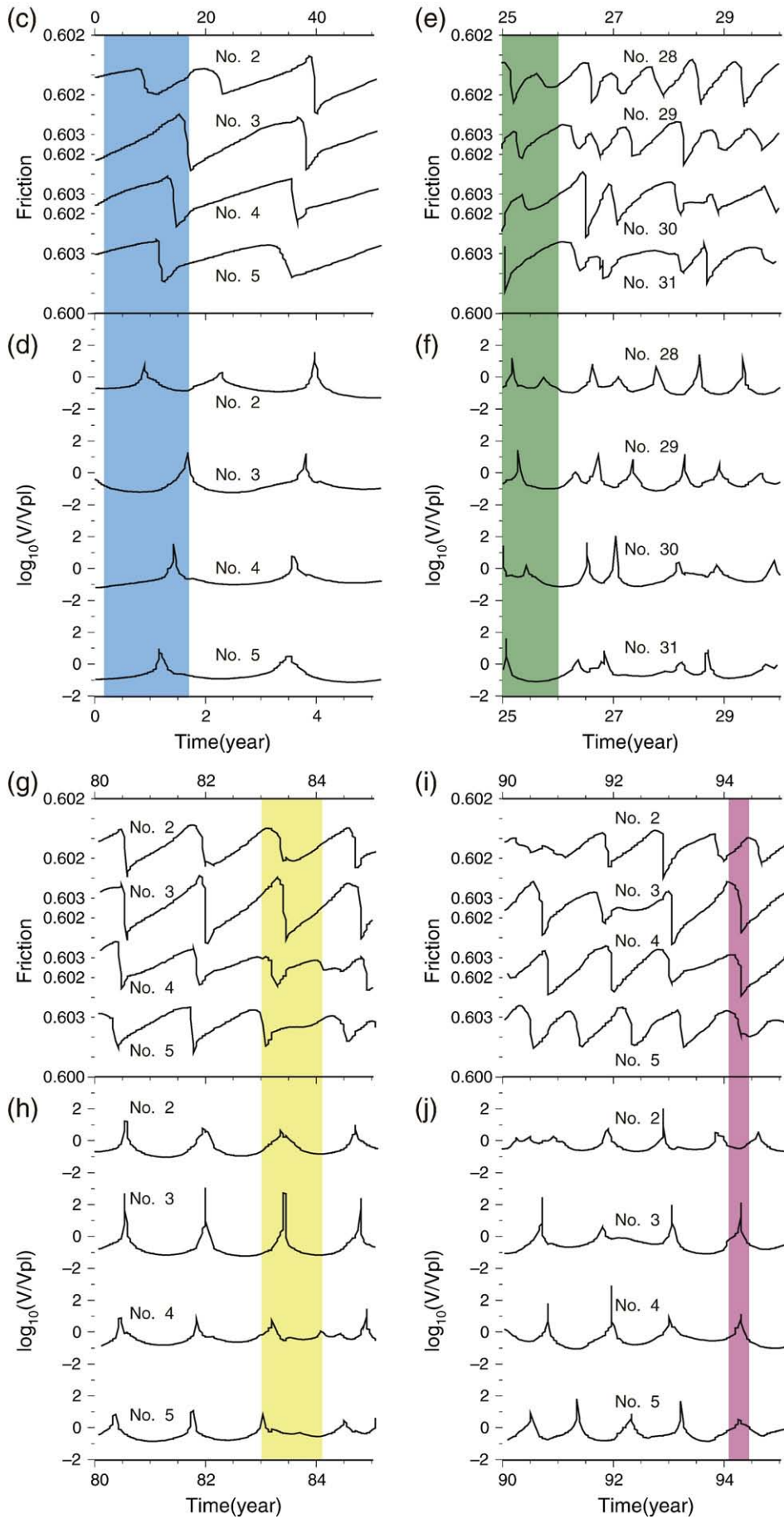


Fig. 2 (continued).

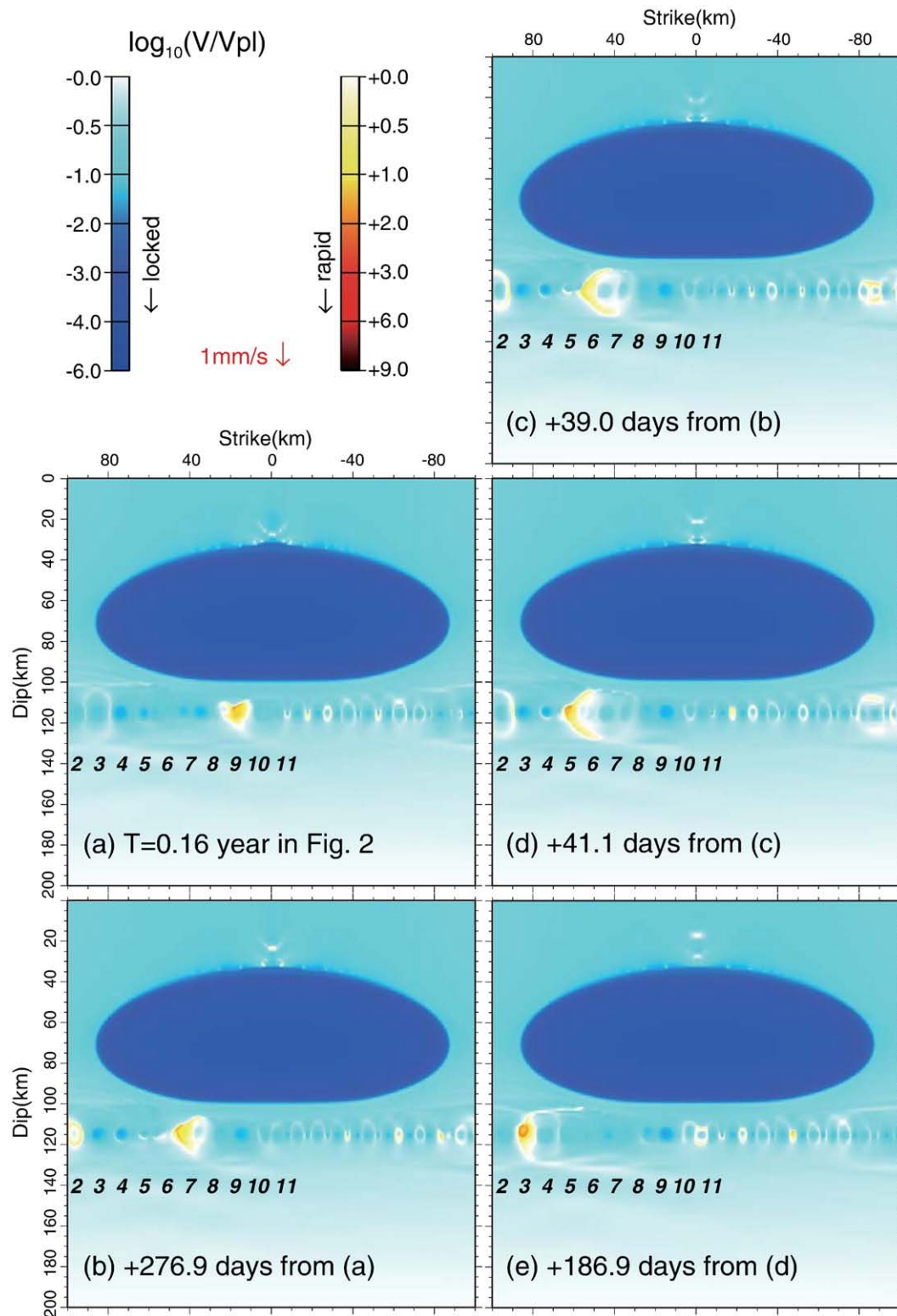


Fig. 3. Snapshots of slip velocity from time 0.16 year as marked by blue color in Fig. 2a–d. Italic numbers under MA are identification of asperities.

explain the physical process of very low-frequency earthquake generation.

4. Summary and discussion

Our simulation represents various types of slow earthquakes, including low-frequency earthquakes and very low-frequency earth-

quakes, due to interaction of asperities aligned along the strike direction, with same size and frictional properties. This result indicates that the interaction between asperities may be a possible mechanism for the generation of low-frequency earthquake and very low-frequency earthquake in the same fault region, without requiring different asperity sizes as previously proposed (Ito et al., 2007).

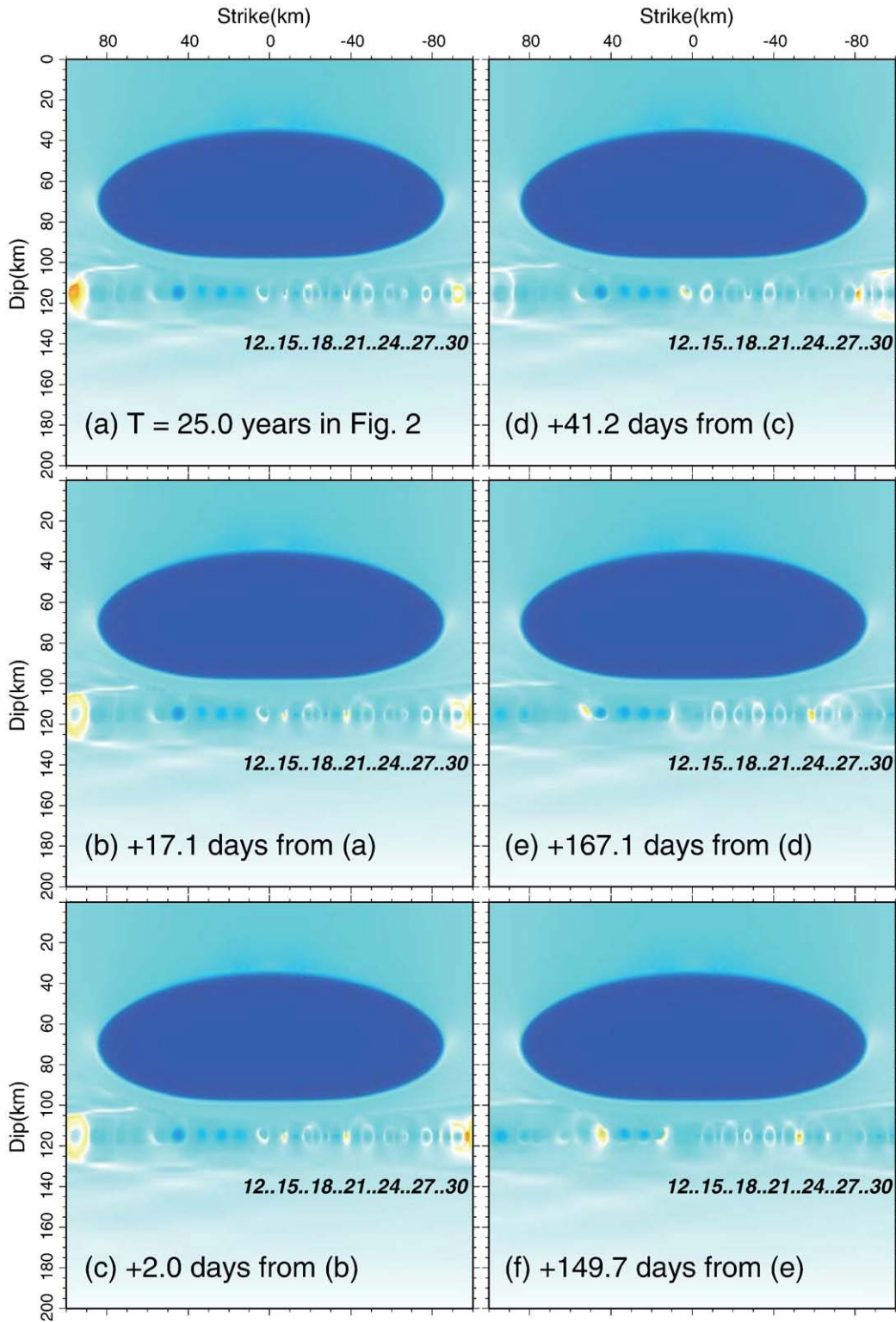


Fig. 4. Snapshots of slip velocity from time 25.0 years as marked by green color in Fig. 2a–b, e–f. Italic numbers under SA are identification of asperities.

Moreover, our simulation also shows unilateral/bilateral propagation and multiple rupture process. We also performed models with longer distance between asperities (more than 5 km for SA and 7.5 km for MA) and found that most of slow earthquakes occurred independently and had weaker variability of slip velocity and stress drop. These results suggest that the interaction effect may be a possible mechanism of low-frequency earthquake migration, alternative to the

fluid movement hypothesis (Obara, 2002), and that the distribution of asperities may be very dense along the strike direction at the depth of around 30 km.

The propagation speed in our model varies in the range 0.03–3 km/day, which is more dispersed than observational results in the range 5–15 km/day (Obara, 2002; Rogers and Dragert, 2003; Obara and Hirose, 2006). Since the propagation speed in our model is

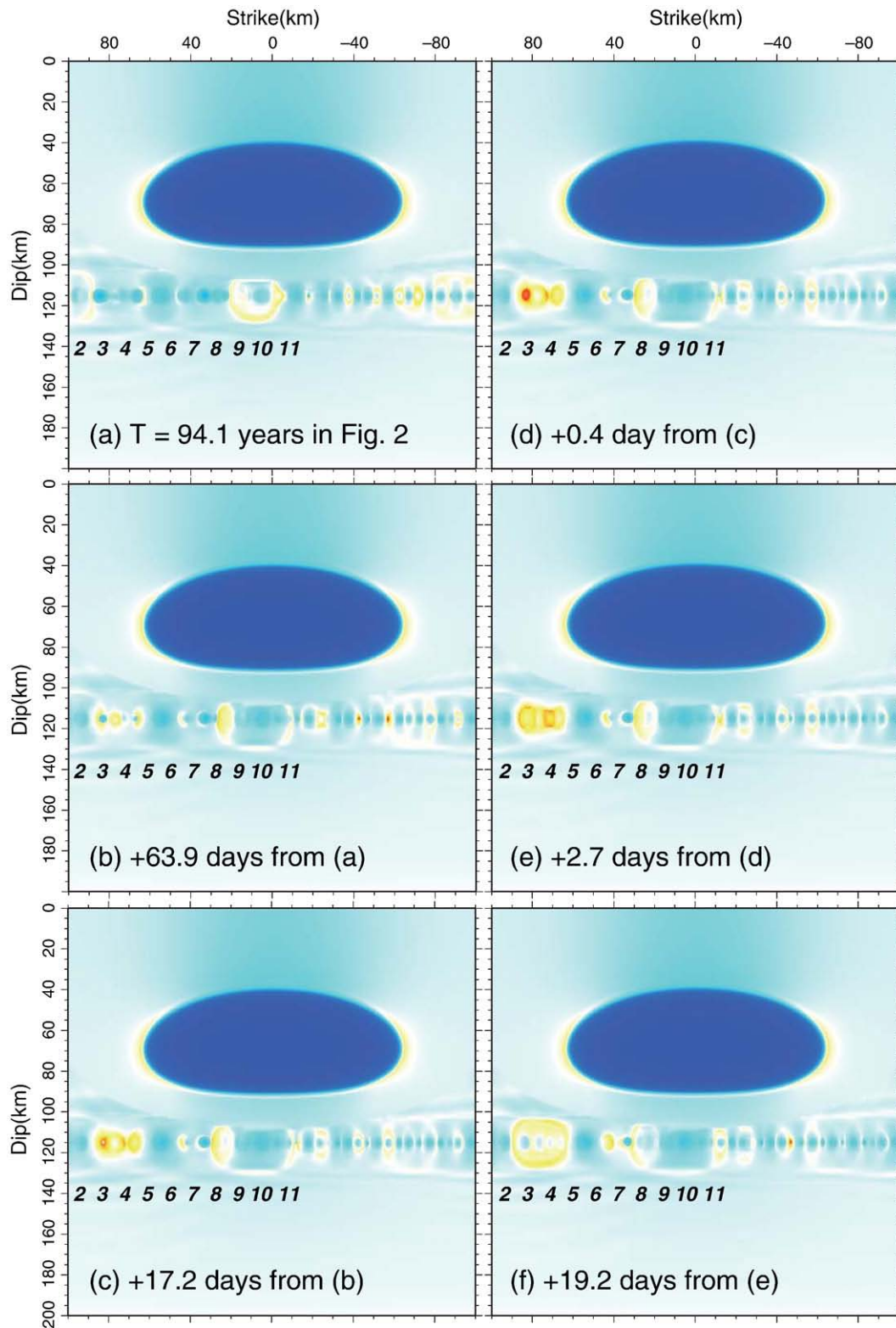


Fig. 5. Snapshots of slip velocity from time 94.1 years as marked by pink color in Fig. 2a–b, i–j. Italic numbers under MA are identification of asperities.

significantly lower than observed, it is necessary for us to explain the propagation speed quantitatively by modifying our model. Ariyoshi et al. (2007b) demonstrated that shorter characteristic distance as well as lower effective normal stress makes afterslip propagation of a large earthquake faster by changing frictional property. However, models with shorter characteristic distance than the original model in

Fig. 1 need heavier computations, especially just before and after giant earthquakes at LA.

From Fig. 2a–b, the recurrence intervals of SA and MA tend to be shorter because slip velocity field around LA becomes higher towards to the preseismic stage of LA in comparison with Figs. 3–6. Ariyoshi et al. (2007a) found that slow earthquakes occur at a

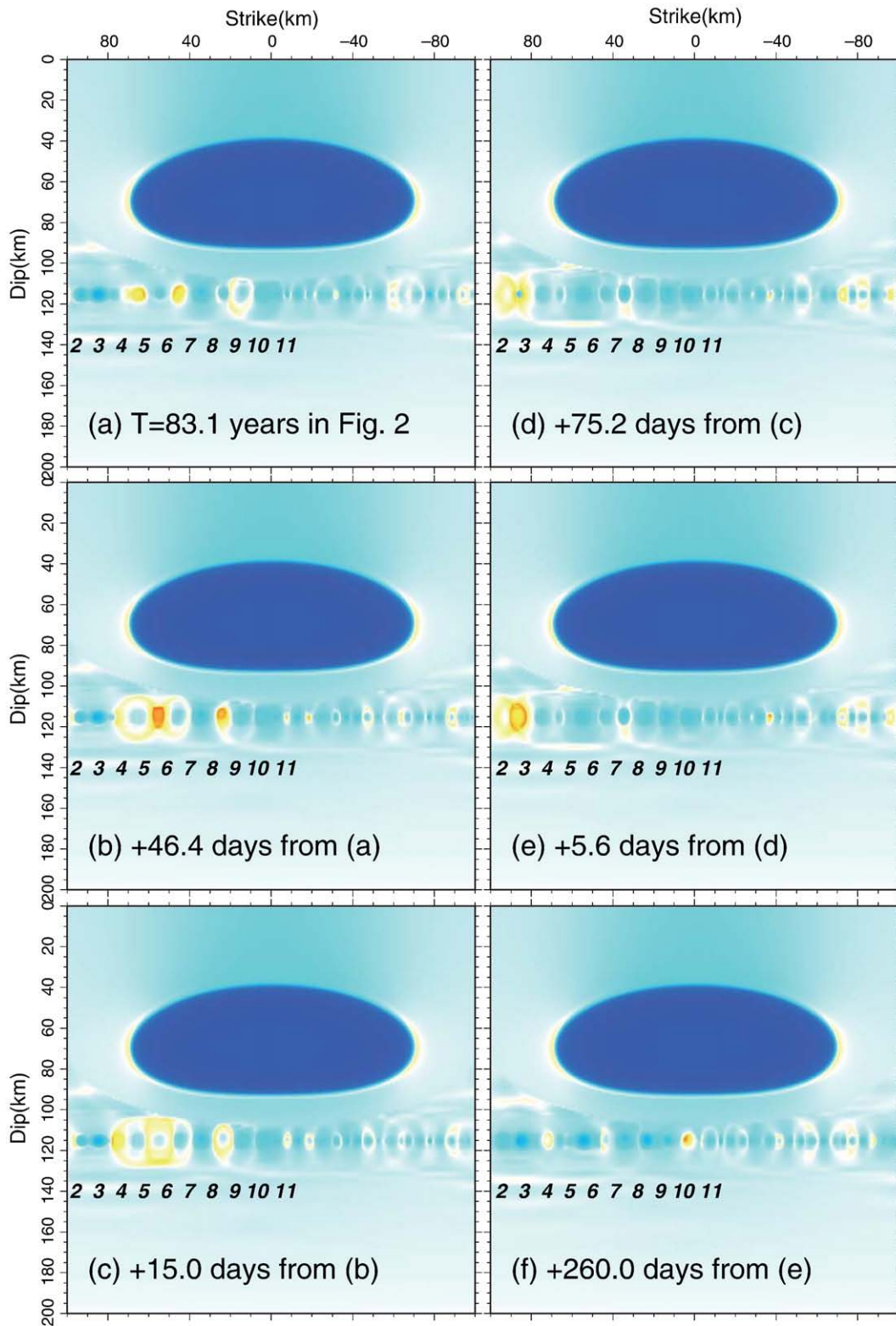


Fig. 6. Snapshots of slip velocity from time 83.1 years as marked by yellow color in Fig. 2a–b, g–h. Italic numbers under MA are identification of asperities.

small asperity in the passage of large postseismic slip, which could be another mechanism of very low-frequency earthquake generation. It is our future study to improve our numerical simulations so as to explain the propagation speed quantitatively and to investigate the change of slow earthquake behavior before and after giant earthquakes in order to find a way to monitor the state of large asperities.

Acknowledgements

Discussion with Dr. Bunichiro Shibasaki was useful to sharpen the target of our simulation. Dr. Kazushige Obara kindly taught us the details of observed low-frequency earthquake behaviors. We thank two reviewers for constructive comments and Dr. M. Santosh and Dr. S. Maruyama for expeditious editorial handling. This study used the

Earth Simulator for our simulations, and the supercomputing resources at Cyberscience Center of Tohoku University for running experimental simulation to improve program codes. This work is supported by DONET program of the Ministry of Education, Culture, Sports, Science and Technology. GMT software (Wessel and Smith, 1998) was used to draw some figures.

References

- Ariyoshi, K., Matsuzawa, T., Hino, R., Hasegawa, A., 2007a. Triggered non-similar slip events on repeating earthquake asperities: results from 3D numerical simulations based on a friction law. *Geophysical Research Letters* 34, L02308.
- Ariyoshi, K., Matsuzawa, T., Hasegawa, A., 2007b. The key frictional parameters controlling spatial variations in the speed of postseismic slip propagation on a subduction plate boundary. *Earth and Planetary Science Letters* 256, 136–146.
- Blanpied, M.L., Marone, C.J., Lockner, D.A., Byerlee, J.D., King, D.P., 1998. Quantitative measure of the variation in fault rheology due to fluid-rock interactions. *Journal of Geophysical Research* 103, 9691–9712.
- Boatwright, J., Cocco, M., 1996. Frictional constraints on crustal faulting. *Journal of Geophysical Research* 101 (B6), 13895–13909.
- Dieterich, J.H., 1979. Modeling of rock friction: 1. Experimental results and constitutive equations. *Journal of Geophysical Research* 84, 2161–2168.
- Hasegawa, A., Nakajima, J., Kita, S., Okada, T., Matsuzawa, T., Kirby, S., 2007. Anomalous deepening of a belt of intraslab earthquakes in the Pacific slab crust under Kanto, central Japan: possible anomalous thermal shielding, dehydration reactions, and seismicity caused by shallower cold slab material. *Geophysical Research Letters* 34 (9), L09305. doi:10.1029/2007GL029616.
- Hirose, H., Hirahara, K., 2002. A model for complex slip behavior on a large asperity at subduction zones. *Geophysical Research Letters* 29 (22), 2068.
- Hirose, H., Obara, K., 2005. Repeating short- and long-term slow slip events with deep tremor activity around the Bungo channel region, southwest Japan. *Earth Planets Space* 57 (10), 961–972.
- Horowitz, F.G., Ruina, A., 1989. Slip patterns in a spatially homogeneous fault model. *Journal of Geophysical Research* 94 (B8), 10279–10298.
- Ide, S., Shelly, D.R., Beroza, G.C., Uchide, T., 2007. A scaling law for slow earthquakes. *Nature* 447, 76–79.
- Ito, Y., Obara, K., Shiomi, K., Sekine, S., Hirose, H., 2007. Slow earthquakes coincident with episodic tremors and slow slip events. *Science* 315, 503–506.
- Kita, S., Okada, T., Nakajima, J., Matsuzawa, T., Hasegawa, A., 2006. Existence of a seismic belt in the upper plane of the double seismic zone extending in the along-arc direction at depths of 70–100 km beneath NE Japan. *Geophysical Research Letters* 33, L24310.
- Kutsukake, T., 2002. Geochemical characteristics and variations of the Ryoke Granitoids, Southwest Japan: petrogenetic implications for the plutonic rocks of a magmatic arc. *Gondwana Research* 5 (2), 355–372.
- Liu, Y., Rice, J.R., 2005. Aseismic slip transients emerge spontaneously in three-dimensional rate and state modeling of subduction earthquake sequences. *Journal of Geophysical Research* 110, B08307.
- Matsuzawa, T., Uchida, N., Igarashi, T., Okada, T., Hasegawa, A., 2004. Repeating earthquakes and quasi-static slip on the plate boundary east off northern Honshu, Japan. *Earth Planets Space* 56, 803–811.
- Miller, M.M., Melbourne, T., Johnson, D.J., Summer, W.Q., 2002. Periodic slow earthquakes from the Cascadia subduction zone. *Science* 295, 2423.
- Mishina, M., 2009. Distribution of crustal fluids in Northeast Japan as inferred from resistivity surveys. *Gondwana Research* 16, 563–571 (this issue).
- Miyazaki, S., Segall, P., McGuire, J., Kato, T., Hatanaka, Y., 2006. Spatial and temporal evolution of stress and slip rate during the 2000 Tokai slow earthquake. *Journal of Geophysical Research* 111, B03409.
- Obara, K., 2002. Nonvolcanic deep tremor associated with subduction in southwest Japan. *Science* 296, 1679–1681.
- Obara, K., Hirose, H., 2006. Non-volcanic deep low-frequency tremors accompanying slow slips in the southwest Japan subduction zone. *Tectonophysics* 417, 33–51.
- Okada, Y., 1992. Internal deformation due to shear and tensile faults in a halfspace. *Bulletin of Seismological Society of America* 82, 1018–1040.
- Perfettini, H., Ampuero, J.P., 2008. Dynamics of a velocity strengthening fault region: implications for slow earthquakes and postseismic slip. *Journal of Geophysical Research* 113, B09411.
- Press, W.H., Flannery, B.P., Teukolsky, S.A., Vetterling, W.T., 1996. *Numerical recipes in Fortran 77: the art of scientific computing*, 2nd edition. Cambridge University Press, New York. 963 pp.
- Rice, J.R., 1993. Spatio-temporal complexity of slip on a fault. *Journal of Geophysical Research* 98 (B6), 9885–9907.
- Rogers, G., Dragert, H., 2003. Episodic tremor and slip on the Cascadia subduction zone: the chatter of silent slip. *Science* 300, 1942–1943.
- Rubin, A.M., Ampuero, J.P., 2005. Earthquake nucleation on (aging) rate and state faults. *Journal of Geophysical Research* 110 (B11), B11312.
- Ruina, A.L., 1983. Slip instability and state variable friction laws. *Journal of Geophysical Research* 88, 10359–10370.
- Savage, J.C., 1983. A dislocation model of strain accumulation and release at a subduction zone. *Journal of Geophysical Research* 88, 4984–4996.
- Shelly, D.R., Beroza, G.C., Ide, S., Nakamura, S., 2006. Low-frequency earthquakes in Shikoku, Japan, and their relationship to episodic tremor and slip. *Nature* 442, 188–191.
- Shibasaki, B., Shimamoto, T., 2007. Modeling of short-interval silent slip events in deeper subduction interfaces considering the frictional properties at the unstable–stable transition regime. *Geophysical Journal International* 171, 191–205.
- Sun, A., Zhao, D., Ikeda, M., Chen, Y., Chen, Q., 2008. Seismic imaging of southwest Japan using P and PmP data: implications for arc magmatism and seismotectonics. *Gondwana Research* 14, 535–542.
- Wang, K., Suyehiro, K., 1999. How does plate coupling affect crustal stresses in Northeast and Southwest Japan? *Geophysical Research Letters* 26, 2307–2310.
- Wessel, P., Smith, W.H.F., 1998. New, improved version of the generic mapping tools released. *EOS Transaction AGU* 79, 579.
- Zhao, D., 2009. Multiscale seismic tomography and mantle dynamics. *Gondwana Research* 15, 297–323.
- Zhao, D., Ohtani, E., 2009. Deep slab subduction and dehydration and their geodynamic consequences: evidence from seismology and mineral physics. *Gondwana Research* 16, 401–413 (this issue).
- Zhao, D., Maruyama, S., Omori, S., 2007. Mantle dynamics of Western Pacific and East Asia: insight from seismic tomography and mineral physics. *Gondwana Research* 11, 120–131.
- Ziv, A., 2007. On the nucleation of creep and the interaction between creep and seismic slip on rate- and state-dependent faults. *Geophysical Research Letters* 34, L15303.